

Previous theoretical work has analyzed the spectral and angular characteristics of PXR generated in mosaic crystals [1]. A recent report (Fiorito, et. al., ref. [2]) described the measurement of parametric X rays (PXR) from a mosaic crystal (pyrolytic graphite) placed in the path of a 90-MeV electron beam. The measured multiple-order spectra were very clear, and some higher orders (up to $n = 8$, $\simeq 37 \text{ KeV}$) had surprisingly high intensities. The present paper reports spectral and angular measurements of PXR from a similar pyrolytic graphite crystal exposed to 900-MeV electrons from the Tomsk "Sirius" synchrotron. This work was performed in order to clarify the

nature of the angular and spectral distributions of PXR from mosaic crystals. The spectral distribution of PXR is interesting because the higher order "modes" can generate tunable narrow bands of hard x-rays.

Generally speaking, PXR generation mechanism tend not to be efficient when $\omega > \gamma\omega_p$, where ω is the radiation frequency, γ is the Lorentz factor of the electron, and ω_p is the electron plasma frequency of the material [3]. With $\gamma\omega_p \simeq 5.4 \text{ keV}$, the Fiorito PXR spectra had features with $\omega_B < \gamma\omega_p$ and $\omega_B > \gamma\omega_p$, where ω_B is the PXR frequency. The present experiment measures similar spectra under conditions where $\omega_B < \gamma\omega_p$ when the spectral and angular distributions of PXR must be described by the kinematical theory of PXR [1].

The angular distribution of PXR emitted at angle $\Theta_D = \pi/2$ is interesting because it has single- and double-lobed characteristics parallel to and perpendicular to the diffraction (or reflecting) plane, respectively. The single-lobe in-plane structure means that single spectral features can be isolated in the output. The double-lobe out-of-plane structure is similar to the angular distribution of transition radiation.

The geometry of the experiment is shown in Fig. 1. The target crystal was pyrolytic graphite (CAPG) 11x6x1 mm³, produced by Union Carbide Corporation. The Bragg angle between incident electron beam and diffraction planes (200) was $\Theta_B = \pi/4$, and the end of the crystal was beveled at 45° in order to minimize edge effects. X rays were measured with a Xe (1 atm., 12 mm cylinder) proportional counter with the angular aperture $1.74 \times 13.9 \text{ mrad}$. The measurements were performed with the internal beam of the Tomsk synchrotron. Further experimental details have been described previously [4].

The zero Bragg angle condition was determined by monitoring channeling radiation (CR) while rotating the crystal in the

electron beam. The channeling radiation intensity peaks when the crystal planes are parallel to the electron trajectory (see Fig. 1a). Furthermore, the intensity versus crystal orientation gives a measure of the mosaicity of the microcrystals in the sample. Figure 2a shows the orientation dependence of CR from the graphite crystal. For highly collimated electron beams, the width FWHM can be defined choosing the maximal value between Θ_L and σ_M , where $\Theta_L = \sqrt{2U/E_e}$ is the Lindhard angle [5], σ_M is the Gaussian half-width of the crystal mosaicity of a sample ($M = D, T, G$ for diamond, tungsten and graphite, respectively), E_e is the electron energy, and U is the maximum value of the continuous plane potential. Figure 2 shows the measured dependence of CR intensity on crystal orientation for the pyrolytic graphite, natural diamond ($\sigma_D \simeq 0.2 \text{ mrad}$), and tungsten ($\sigma_T \simeq 1 \text{ mrad}$) crystals. The data in Fig. 2a can be used to estimate the mosaicity of the graphite sample: $\sigma_G \simeq 3.4 \text{ mrad}$ ($\sigma_G \simeq FWHM/2.36$).

After using CR to orient the crystal planes parallel to the electron beam the crystal was rotated to a $\pi/4$ Bragg angle (as in Fig. 1b). The detector window (slit) was perpendicular to the scattering plane. The resulting PXR spectrum in Fig. 1c shows peaks corresponding to $n = 2, 3, 4$ at about 5.0, 7.5, and 11.0 keV, respectively. These energies agree, within experimental uncertainty, with theoretical predictions according to the well known formula [3]:

$$\omega_B = \frac{\pi n \sin \theta_B}{a(1 - \cos \theta_D)} \quad (1)$$

where a is the spacing between reflecting planes and θ_D is the detection (or emission) angle. Table I summarizes these results. The small peak at about 1.5 KeV is an artifact caused by electronic noise. The spectrum in Fig. 1c is not corrected

for the spectral response of the detector.

According our estimations, the detector efficiency was 1.45% at 7.5 KeV and 25.6% at 5.2 KeV, and 38, 0% at 10.4 KeV.

TABLE 1

Reflection order, n	2	3	4
E_{exp}, KeV	5.0 ± 0.3	7.5 ± 0.5	11.0 ± 0.5
E_{theor}, KeV	5.2	7.8	10.4

Figure 3 shows the dependence of PXR yield at 90 degrees on crystal rotation (the detector position was the same as during spectral measurement). The maximum corresponds to an angle $\Theta_B = 44^\circ 28'$, indicates accurate orientation of the crystal. Because the intrinsic PXR width is very small, the width of the peak in Fig. 3 is dominated by the crystal mosaicity. Here, the width, $FWHM \simeq 10 \text{ mrad}$, is consistent with that observed with the CR measurement in Fig. 2a.

Finally, Fig. 4 shows measurements of angular distribution of the (600) reflection in the vertical plane (perpendicular to the plane of incidence). Here, the detector slit was parallel to the diffraction planes.

Similar previous measurements [6] of (220) reflection PXR from a diamond target have produced results that agreed well with the kinematic PXR theory [7]. This theory expresses the angular distribution of PXR, relative to the Bragg direction, as:

$$\frac{dN}{(d\Theta_x d\Theta_y)} = F(\Theta_x, \Theta_y) = const \frac{\Theta_x^2 \cos^2 2\Theta_B + \Theta_y^2}{(\Theta_x^2 + \Theta_y^2 + \Theta_{ph}^2)^2}, \quad (2)$$

Here, the definition of Θ_{ph}^2 has been expanded to include a contribution that describes the effect of multiple scattering of electrons in the target: $\Theta_{ph}^2 = \gamma^{-2} + \omega_p^2/\omega_B^2 + \Theta_{MS}^2$, where

Θ_{MS}^2 is the multiple scattering angle. As mentioned above, eq 2 with $\Theta_B = \pi/4$ describes the "two-lobe" distribution with maxima shifted relative Bragg direction to the angles $\Theta_{y,max} = \pm\Theta_{ph}$, dashed line in Fig.4. The present analysis estimates the influence of multiple scattering by treating the target as the sum of a number of thin layers, whose contributions are integrated to obtain the overall angular distribution, F_{MS} .

The present PXR angular distributions are dominated by the graphite crystal mosaicity. The influence of mosaicity is modeled by a description in reference [8] which writes the distribution of mosaicity angles as:

$$P(\alpha_x, \alpha_y) = P(\alpha_x)P(\alpha_y) = \frac{1}{2\pi\sigma_M^2} \exp\left(-\frac{\alpha_x^2}{2\sigma_M^2}\right) \exp\left(-\frac{\alpha_y^2}{2\sigma_M^2}\right). \quad (3)$$

where α_x, α_y are deviation angles of mosaic element from average direction of reciprocal lattice vector, respectively. For the present experiment, the variation of Bragg direction for each mosaic element, leads to deviation of Bragg direction for emitted photons, relative which the angles Θ_x, Θ_y in equation (2) are defined:

$$(\Theta_D)_x \simeq 2\alpha_x, \quad (\Theta_D)_y \simeq -2\alpha_y \sin\Theta_B. \quad (4)$$

Therefore, the angular distribution of PXR can be described by:

$$\frac{dN_M}{(d\Theta_x d\Theta_y)} = \int d\alpha_x \int d\alpha_y P(\alpha_x)P(\alpha_y) F_{MS}(\Theta_x - 2\alpha_x, \Theta_y + 2\alpha_y \sin\Theta_B). \quad (5)$$

Figures 3 and 4 compare the results of calculations of Eq. (5) with the data. As a simplification, the calculations used a

one-dimensional angular distribution over coordinate α_x or α_y , respectively (since the detector window was the split with one side much greater than other) and taking into account multiple scattering of electrons and the detector aperture

The results in Figs. 3 and 4 do not show good agreement between experiment and calculations, because the results of calculations give greater values for angular widths of PXR distributions.

In conclusion, we find that:

a) The main features of the present data are consistent with kinematical theory of PXR with taking into account the crystal mosaicity [7].

b) When $\sigma_M \simeq \Theta_{ph}$, the "strong" mosaicity doesn't lead to significant broadening of angular distribution; and therefore the use of mosaic crystals does not lead to a decrease of PXR brilliance. Indeed, with two orders increase of mosaicity (compare, σ_C and σ_M) only two times increase of angular width was observed.

c) A single-parameter phenomenological model of PXR does not produce accurate descriptions of the angular distribution of PXR from mosaic crystals. Here, the width of the mosaic distribution (the single parameter) was determined by measurements of CR.

The further detailed experimental studies are necessary to clarify the features of PXR in mosaic crystals.

REFERENCES

1. A.M.Afanas'ev, M.A.Aginyan, Zh.Exper.Teor.Fiz.V.74 No 2 (1978) 570 (Sov.Phys. JETP 47 (1978) 300) SPHJA
2. R.B.Fiorito, D.W.Rule, X.K.Maryama et al., Phys.Rev.Lett.V.71 (1993) 704
3. M.L.Ter-Mikaelian, High Energy Electromagnetic Processes in Condensed Media (Wiley-Interscience, New York, 1972)
4. A.N.Didenko, B.N.Kalinin, S.Pak et al, Phys. Lett.A, V.110 No 3 (1985) 177
5. See, for example in : Relativistic Channeling, R.Carrigan ed., 1985
6. Yu.N.Adishchev, et al., Zh.Exper.Teor.Fiz. V.93 No 6 (1987) 1942 ZETFA
7. I.D.Feranchuk and A.V.Ivashin, J.Phys.(Paris) V.46 (1985) 1981 JOPON
8. D.W.Rule, in: Proceedings of Intern.Symposium on Radiation of Relativistic Electrons in Periodical Structures, Tomsk, 6-10 September 1993, to be published.

FIGURE CAPTIONS

- Fig.1 The experimental layout for CR measurements (a), for PXR measurements (b) and measured PXR spectrum (c) for $\Theta_B = \pi/4$.
- Fig.2 The measured orientation dependencies of CR from graphite (a), from natural diamond (b) and from tungsten (c). The crystal thickness $T(mn)$ and channeling planes are indicated.
- Fig.3 Experimental (crosses) and calculated orientation dependencies $R(\Theta_B)$ of PXR photons ($n = 3, \hbar\omega_B = 7.8KeV$). Solid line - calculation with taking into account the crystal mosaicity; dashed line - calculation without taking into account the mosaicity, into the given detector aperture.
- Fig.4 Experimental (crosses) and calculated angular distributions $R(\Theta_y)$ of PXR photons ($n = 3, \hbar\omega_B = 7.8KeV$). Solid line - calculation with taking into account the crystal mosaicity; dashed line - calculation without taking the mosaicity, into the given detector aperture.

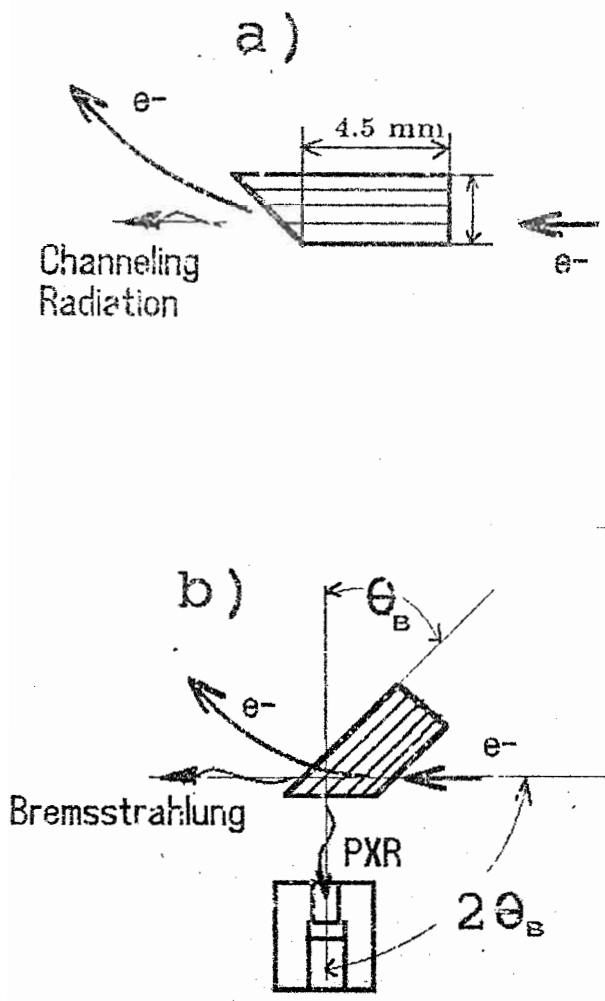


Fig. 1a,b

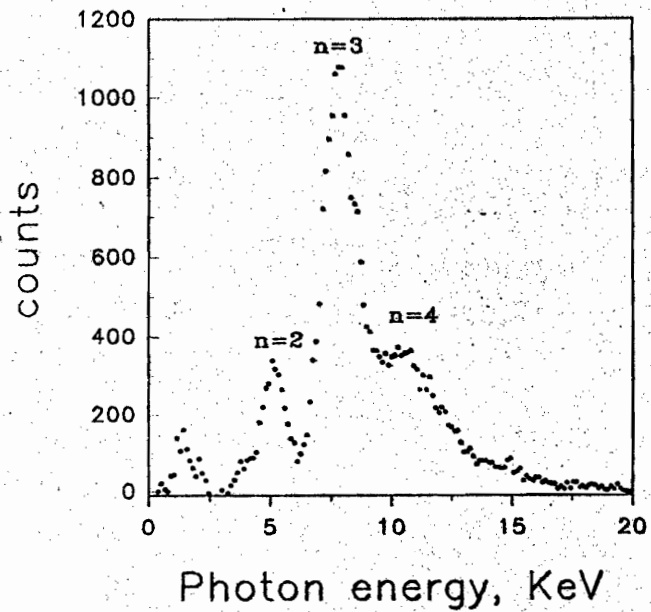


Fig. 1c

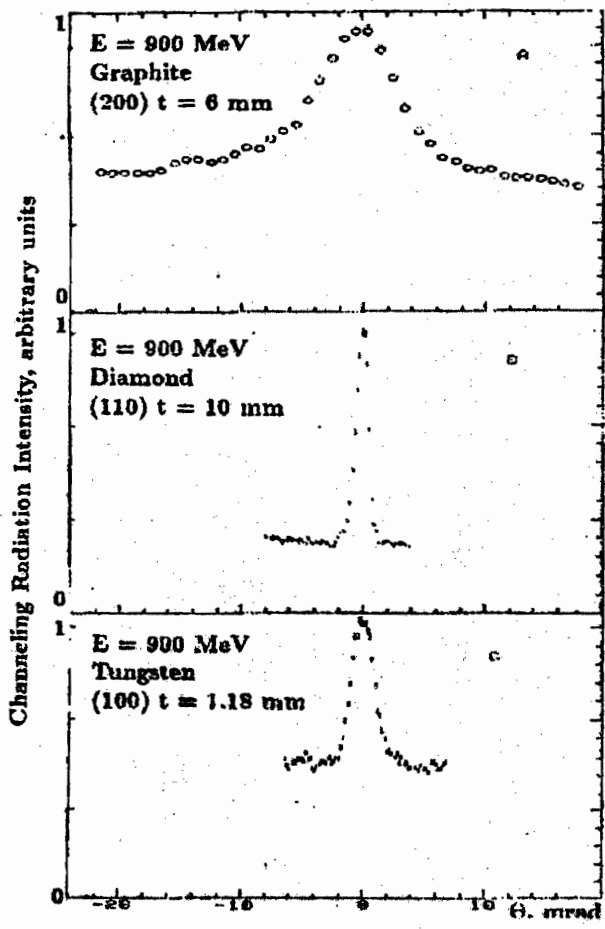


Fig. 2

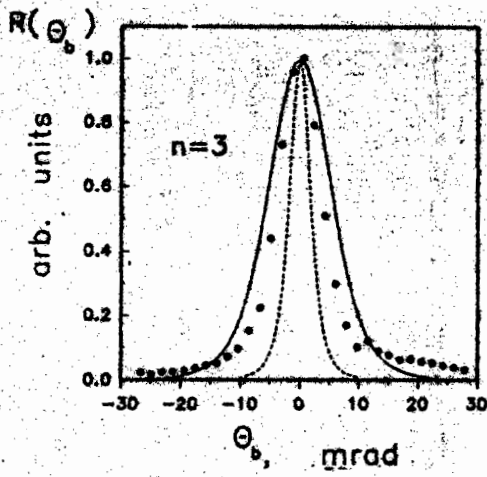


Fig. 3

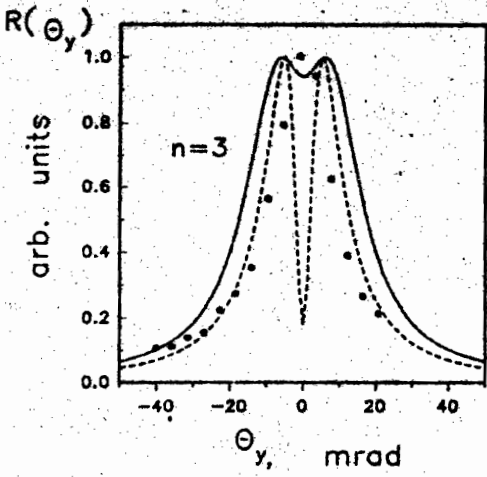


Fig. 4